

Simulation of Imaging Atmospheric Cherenkov Telescopes with CORSIKA and sim_telarray

Konrad Bernlöhr^{a,b}

^a*Max-Planck-Institut für Kernphysik, Postfach 103980, 69029 Heidelberg,
Germany*

^b*Institut für Physik, Humboldt-Universität zu Berlin, Newtonstraße 15, 12489
Berlin, Germany*

Abstract

Imaging Atmospheric Cherenkov Telescopes (IACTs) have resulted in a breakthrough in very-high energy (VHE) gamma-ray astrophysics. While early IACT installations faced the problem of detecting any sources at all, current instruments are able to see many sources, often over more than two orders of magnitude in energy. As instruments and analysis methods have matured, the requirements for calibration and modelling of physical and instrumental effects have increased. In this article, a set of Monte Carlo simulation tools is described that attempts to include all relevant effects for IACTs in great detail but aims to achieve this in an efficient and flexible way. These tools were originally developed for the HEGRA IACT system and later adapted for the H.E.S.S. experiment. Their inherent flexibility to describe quite arbitrary IACT systems makes them also an ideal tool for evaluating the potential of future installations. It is in use for design studies of CTA and other projects.

Key words: Air showers, Imaging atmospheric Cherenkov technique, Gamma-ray astronomy

PACS: 02.70.Uu, 07.05.Tp, 95.55.Ka

1 Introduction

Any simulation of the IACT technique consists of two major components: the development of the extensive air showers and emission of Cherenkov light by

Email address: Konrad.Bernloehr@mpi-hd.mpg.de (Konrad Bernlöhr).

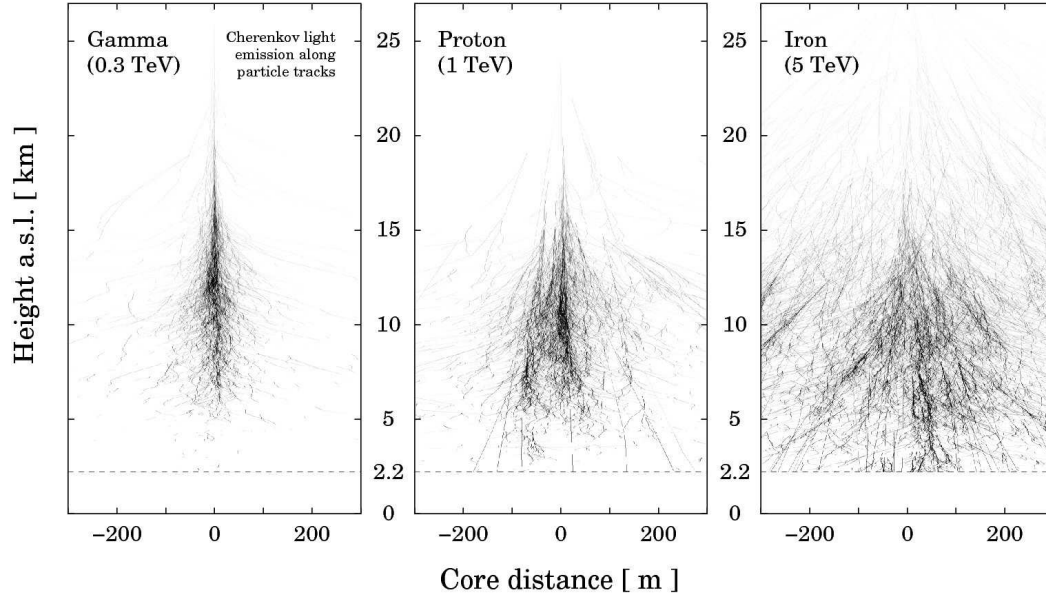


Fig. 1. Cherenkov light production in CORSIKA for different primary particle examples in simulations for a site at 2200 m altitude. Darkness of the particle tracks shown increases with increasing emission of Cherenkov light.

the shower particles as one part and the detection of this light and recording of signals by the instrument as the other part. While earlier simulation tools used to come with a rather primitive description of the instrumental response included with the shower simulation, the simulation tools described here separates these parts into distinct programmes. This allows for enhanced flexibility in the implementation and sharing of components in the community.

The first major component is based on the CORSIKA program [1]. A first implementation of Cherenkov light in CORSIKA, by M. Rozanska, F. Arqueros, and S. Martinez, implemented a rectangular grid of detectors – for the non-imaging HEGRA AIROBICC instrument [2]. The current implementation, by the author of this paper and with contributions by others, unified the originally separate functions for Cherenkov emission by electrons/positrons and by other particles, improved its efficiency and accuracy, and added a great level of flexibility. The CORSIKA code base includes different output formats now, some more generic and some dedicated to specific experiments. Only the most generic of these, the IACT option also developed by us, will be covered here. With the IACT option, a telescope or other Cherenkov detector in CORSIKA is defined by a fiducial sphere containing the reflector or detector.

The second major component, termed `sim_telarray` or – in its current incarnation for the H.E.S.S. experiment [3] – `sim_hessarray`, implements all the details of the detectors. This includes optical ray-tracing of the photons, their registration by photomultiplier tubes, switching of discriminators or comparators at the pixel level and at the telescope trigger level, as well as dig-

itization of the resulting signals. Since `sim_telarray` is highly efficient and, in a typical configuration, requires only a small fraction of the CPU time needed for the shower simulation, it is usually run several times in parallel, reading directly from a common output pipe of the CORSIKA IACT option. Each instance might correspond to a different viewing direction, a different atmospheric transmission, or even a completely different mirror and camera definition.

2 CORSIKA and the IACT option

2.1 Cherenkov light production in CORSIKA

Cherenkov light production in CORSIKA (see Figure 1) with its various options¹ (like IACT, ATMEXT, CEFFIC, CERWLEN, ...) has to be enabled before compilation (see [4] for details). This results in a call to the Cherenkov subroutine CERENK for each track segment of charged particles as they are handled by the CORSIKA particle transport code. The transport code takes care of possible interactions, decay, multiple scattering, bending in the geomagnetic field, and ionization energy loss. As far as Cherenkov light production is concerned, each straight track segment is defined by start and end point as well as by the initial and final energy of the particle (assuming continuous energy loss), and its mass and charge.

Since the track segments can have lengths up to several kilometres at high altitudes, the Cherenkov emission subroutine in CORSIKA has to take care of changes in the index of refraction of the air as well as of the change in velocity of the particle. Track segments in CORSIKA are generally shorter when Cherenkov light production is enabled, in particular with the IACT option, where typical multiple scattering angles and bending in the geomagnetic field should be smaller than the pixel scale in the cameras. Too long track segments could result, for example, in too sharp muon rings or even a shift in

¹ CORSIKA options discussed in this paper include:

ATMEXT: atmospheric extension, providing tabulated atmospheric profiles to all CORSIKA variants and refraction to the Cherenkov light.

CEFFIC: Very simple treatment of atmospheric transmission, mirror reflectivity, and quantum efficiency in CORSIKA itself.

CERENKOV: the master switch for enabling Cherenkov emission. Without IACT option, a rectangular detector array is simulated.

CERWLEN: the index of refraction and, thus, the emission angle depends on the wavelength.

IACT: the detectors are defined individually as fiducial spheres and the machine-independent output data format readable by `sim_telarray` gets used.

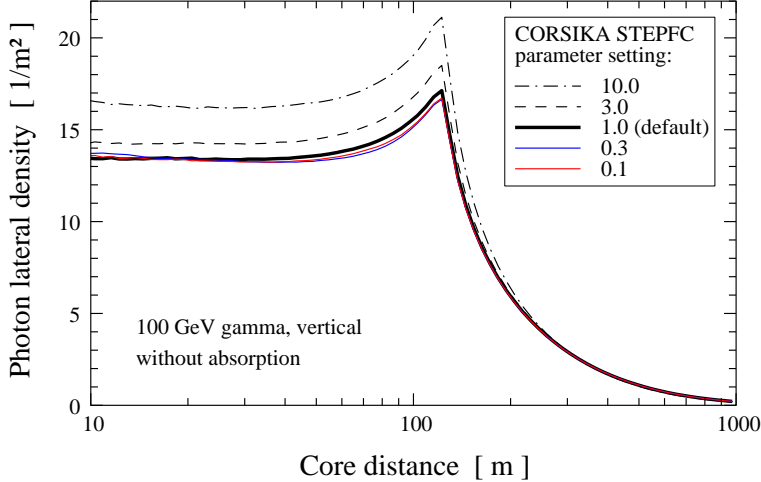


Fig. 2. Average lateral distribution of 300-600 nm Cherenkov light in simulations of vertical 100 GeV gamma-rays for a site at 2200 m altitude, with different settings of the EGS step length parameter STEPFC. Too long step lengths result in a systematic excess of light inside the *light pool* ($r < 120$ m).

the shower maximum. It has been verified that the reduced step lengths with the IACT option (compared to those used in CORSIKA without Cherenkov light production and STEPFC=1.0) do not change the amount of Cherenkov light or its average lateral distribution in any noticeable way, i.e. well below 1 percent.

The STEPFC parameter of CORSIKA could be used to change step lengths of gammas and e^\pm relative to the default settings in EGS [5], which correspond to STEPFC=1.0. While longer step lengths could be used to improve the processing speed, they result in a systematic excess of Cherenkov light by about 20% for STEPFC=10 (see Figure 2). It is reassuring to find that further reductions of step lengths (e.g. STEPFC=0.1) will not result in another systematic change. The question of proper step lengths is certainly an important issue for any shower simulation program – for CORSIKA the built-in default appears to be just the right choice.

While accurate modelling of the showers is perhaps the prime objective in CORSIKA, efficiency is important as well. The efficiency aspect is quite important in the case of the Cherenkov emission subroutine since most of the CPU time is spent there. For many applications, the most important performance gain is achieved by the fact that Cherenkov photons are not simulated one by one but in *bunches*. This concept of bunches was already present in the original implementation [2], with an automatically adapted bunch size as a function of the energy of the primary particle, optimized for the AIROBICC experiment.

For imaging telescopes, an automatic selection of bunch sizes is not so easy.

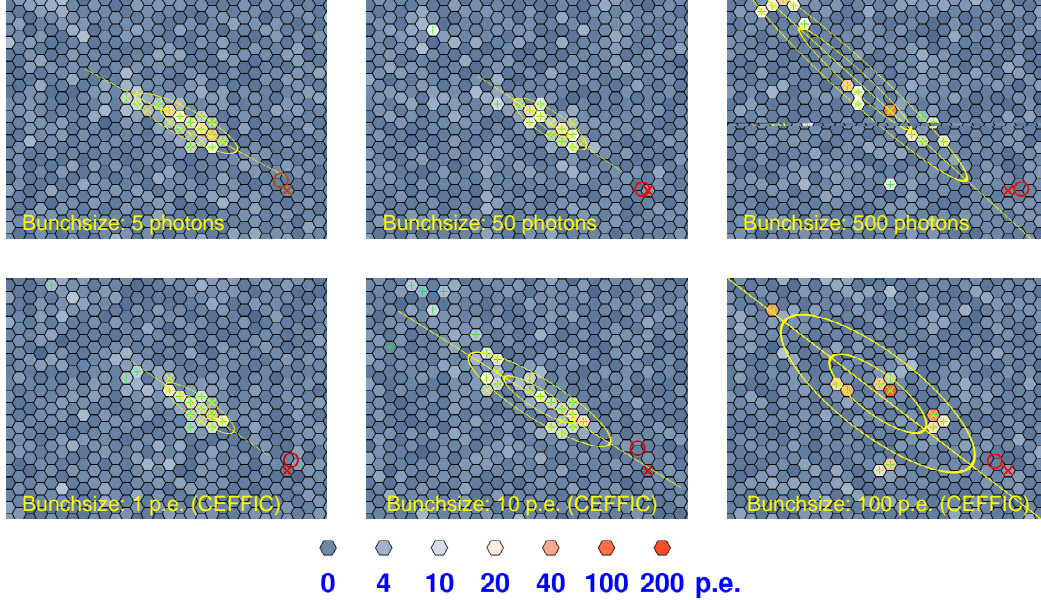


Fig. 3. The effect of different bunch sizes on the image obtained with simulated IACTs. All samples show the same $1.8^\circ \times 1.35^\circ$ part of the field-of-view of a 24 m telescope looking at a 62 GeV γ -ray shower from 117 m core distance. The red cross in each panel indicates the true direction of the incident γ -ray (for other symbols see also Figure 14). The colour scale at the bottom indicates the intensities found in each 0.07° pixel, in units of the average intensity from single photo-electrons (p.e.). Top row: No CEFFIC option, atmospheric transmission and photon detection handled only by `sim_telarray`; left to right: bunch sizes of 5, 50, and 500 (recommended: 5 to 10). Bottom row: With CEFFIC option, detection efficiency applied in CORSIKA: bunch sizes of 1, 10, and 100 (recommended: ≤ 1). Bunch sizes in the left column are small enough to show the actual smooth image, in the middle column artificial fluctuations are already apparent, and in the right column the artificial fluctuations dominated over the true fluctuations in the shower.

Showers induced by high-energy primaries can be detected from large distances while less energetic showers are typically only detected in the region of the almost uniformly illuminated central *Cherenkov light pool*. The optimum bunch size is highly dependent on the detector configuration and best defined by the user in the CORSIKA *inputs* file. See [4] for instructions. Too low values are always safe, but inefficient, while too high values will result in artificial image fluctuations, as illustrated in Figure 3. In a typical configuration with conventional PMTs, a bunch size of 5 to 10 for a wavelength range from 250 to 700 nm should be fairly safe without the CEFFIC option. With the CEFFIC option, where the detection efficiency is included in CORSIKA itself instead of the detector simulation, bunch sizes above one can generally not be recommended.

For a given bunch size, the track segment is sub-divided into steps such that in each step one photon bunch is emitted into a random direction on the Cherenkov cone. The actual size of each bunch and the Cherenkov cone open-

ing angle, defined by $\cos \theta = 1/(\beta n)$, depend on the index of refraction n and the velocity $v = \beta c$ of the particle at the emission point. The wavelength λ of the photons is usually unspecified (unless the CEFFIC or CERWLEN options are used) and may be randomized by the detector simulation to follow the $1/\lambda^2$ distribution in the predefined wavelength range.

Where even more detailed simulations are desired, a random wavelength can be selected in CORSIKA and the wavelength dependence of the index of refraction (see Figure 4) taken into account to determine the emission angle and the amount of light, i.e. bunch size. This level of detail is not normally needed and has a significant impact on performance, and is therefore only enabled on request (CERWLEN option). Normally, the index of refraction n is assumed independent of wavelength and should correspond to an effective wavelength, by default 400 nm. Depending on the configured atmospheric profile, the refractivity $n - 1$ is assumed proportional to the density of the air or interpolated from a table where the dependence on humidity and temperature may be included, typically based on radiosonde data for the site in question.

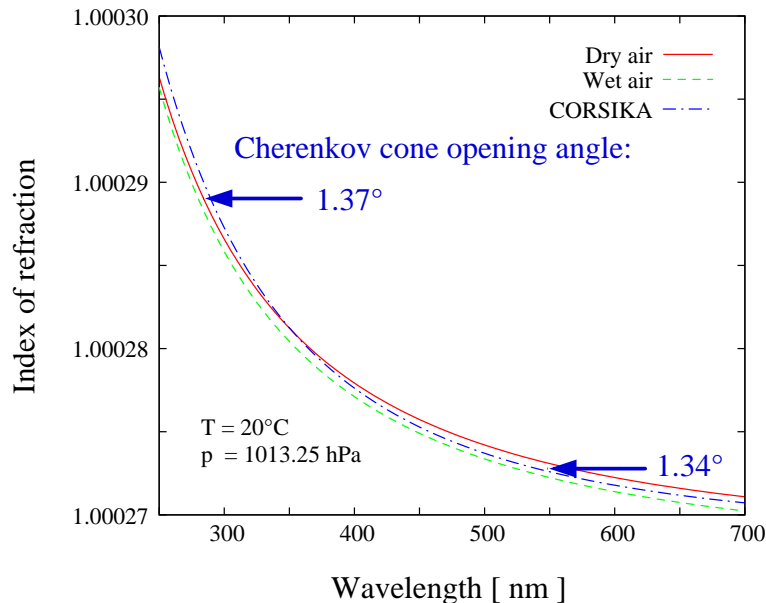


Fig. 4. Wavelength dependence of the index of refraction [6] and its approximation in CORSIKA with the CERWLEN option. The index of refraction as used in CORSIKA typically corresponds to a wavelength of 400 nm. Also shown is the Cherenkov emission angle for a very fast particle under normal sea-level conditions. Maximum opening angles are 1.37° and 1.34° for 300 and 550 nm, respectively, under the given conditions.

2.2 The IACT/ATMO package

The original Cherenkov light implementation in CORSIKA itself was designed to match a rectangular detector array on a horizontal plane. This doesn't allow to match most actual or non-horizontal detector layouts. For large zenith-angle observations, the concept of horizontally flat detectors will even have difficulties with rectangular telescope arrays.

An extension package for CORSIKA, written in the C language, overcomes these limitations. The IACT/ATMO package, together with its corresponding interfaces in CORSIKA, serves several purposes: the geometry of an IACT array can be matched to actual configurations, use of a machine- and compiler-independent data format, use of tabulated atmospheric profiles, and taking atmospheric refraction into account.

An *array* of telescopes or other detectors is defined by the (x_i, y_i, z_i) positions of the centres and the radii r_i of any number of fiducial spheres (currently limited to 1000 in CORSIKA input handling). For a typical IACT the position would best correspond to the intersection of altitude and azimuth axes and the radius would be large enough to enclose the whole reflector. No other properties of the instrument are required in this part of the simulation. For efficient use of the CPU time invested in shower and Cherenkov light simulation, the defined array can be re-used multiple times for each shower at random displacements with respect to the nominal shower core. By default, a circle of given radius $R_{c,\max}$ will be uniformly covered. Depending on the CORSIKA compile-time configuration this can either be a circle in the horizontal *detection plane* as used in CORSIKA without IACT option or in the *shower plane* perpendicular to the direction of the primary particle and projecting them back to the detection level.

Non-uniform coverage is optionally available for implementation by the user. This could be used, for example, for generating low energy showers over a smaller core distance range than high energy showers. Event weights, which are then needed for the reconstruction of spectra, are kept in the provided data format. In the more general case, the non-uniform coverage can support variance reduction schemes for specific questions, i.e. reducing the variance in some resulting number (like the trigger rate, for example) for a given number of showers – or reducing the number of showers required for a given variance. Usually, preference has to be given to the core positions more likely resulting in a trigger, in order to achieve that (thus often called *importance sampling* [7]) – but the optimum distribution depends on the question and detector details and cannot be generalised.

The nominal core position in CORSIKA is along a straight line on the original

direction of the primary particle from its starting position at the assumed top of the atmosphere – typically 100 to 120 km high. Low-energy charged particles, e.g. electrons of a few GeV, suffer substantial bending in the geomagnetic field before their first interaction. For electrons detectable with large IACTs the deflection can approach $R_{c,\max}$ and would affect detection probabilities even under assumption of an isotropic background. The deflection is therefore compensated in the IACT/ATMO package.

Since the possible intersection of each photon path with many spheres would be very CPU intense, a rectangular grid at the detection level is set up and each sphere is linked to one or more of the grid cells as illustrated in Figure 5. Only spheres linked to the grid cell, where a photon bunch arrives, are checked for possible intersections. This scheme is very effective and the CPU time required for accumulating photon bunches hitting any detector is generally negligible. In order to reduce memory requirements, a thinning scheme can set in when too many bunches get collected for a telescope, allowing for high dynamic range simulations. In this thinning scheme, similar to thinning of particles in CORSIKA, the number of bunches is reduced but the number of photons in each of the remaining bunches is increased in compensation.

The photon bunches intersecting any of the detector spheres in any of the randomly displaced array instances are recorded in a machine- and compiler-independent, flexible data format, termed *eventio*, which was originally developed for other purposes [8, 9]. Photon bunches in this format can have an unspecified or a specific wavelength, with negative wavelengths indicating that detection efficiencies were already applied (CEFFIC option, bunches corresponding to photo-electrons). The output can be written to file, with optional automatic compression, or it can be piped into another program, either the telescope simulation directly or into an adapter program which in turn pipes the output into several different telescope simulations. This way, different telescope configurations, different offset angles of the telescopes with respect to the source, and different atmospheric transmission models can be simulated at the same time. Hundreds of shower simulations, with thousands of telescope simulations, can be processed in parallel on a large computer cluster without running into any I/O bottlenecks.²

Another aspect of the IACT/ATMO package, supporting the CORSIKA option ATMEXT, is the possibility to provide tabulated atmospheric profiles. These include the density, the atmospheric thickness, and the effective index of refraction as a function of altitude. Such a table would typically be derived

² With little more than 10 telescope simulations reading CORSIKA data from the same network-mounted RAID array of hard disks, the I/O bandwidth would be saturated. Piping CORSIKA data directly into `sim_telarray`, hundreds of computer nodes may be running 10 telescope simulations each without running into I/O limitations.

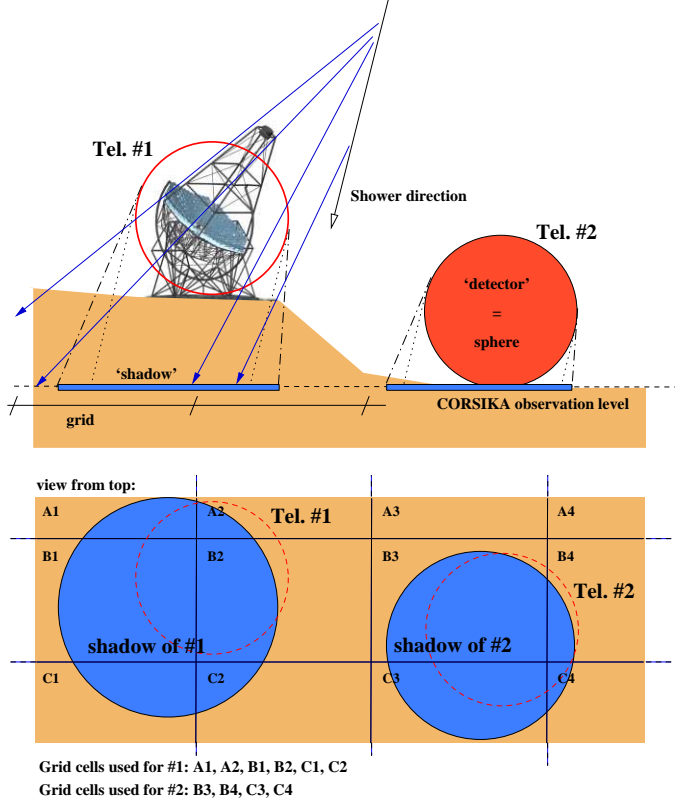


Fig. 5. Definition of grid cells at the detection level to which a detector sphere gets linked for detailed inspection of intersections of photon bunches with the sphere. The *shadow* of a sphere is large enough to include all Cherenkov light emitted up to 10 degrees from the shower direction and intersecting the sphere. For detectors near the CORSIKA observation level even most light emitted at larger angles would be recorded. Some rays at extremely large angles not relevant for IACTs (but perhaps for fluorescence detectors) could go unnoticed for efficiency reasons.

from radiosonde data for the site in question or from atmospheric models. Since the EGS4-based part of CORSIKA cannot interpolate from this table but makes use of several atmospheric layers with piece-wise exponential or (in the top layer) a linear density profile, the corresponding parameters are fitted simultaneously to the atmospheric thickness and density columns at program start-up. Where suitable, the table values are interpolated by taking advantage of the close to exponential density profile.

Since systems of IACTs can achieve an accuracy on the level of a few arc seconds in the positions of point-like sources, atmospheric refraction of Cherenkov light has to be taken into account as well [10]. The refraction correction is provided by the IACT/ATMO package when the CORSIKA option ATMEXT is enabled. It affects the arrival direction, the arrival position, and the arrival time at the CORSIKA detection level. These corrections are evaluated once by numerical integration and then interpolated as functions of starting altitude and zenith angle. Fortunately, the differential refraction, i.e. the dependence

on wavelength, is not relevant yet for the current systems of IACTs.

Scattering of Cherenkov light is optionally available, including both Rayleigh and Mie scattering. However, this requires preparation of special data files, is very CPU-intense, and thus not normally used. In addition, scattered Cherenkov light is irrelevant within the short integration times of IACTs [10]. The scattering option is therefore not included in the package version distributed with CORSIKA but available on request only.

3 The `sim_telarray` telescope simulation package

3.1 Overview

The `sim_telarray` package was originally developed for the HEGRA IACT system [9]. In this early implementation, many aspects were still hard-wired, e.g. that the telescope trigger would be a next-neighbour trigger with a pixel logic corresponding to discriminators with immediate switching and sharp rising and falling edges of the signal. For the design issues with H.E.S.S. and future telescope systems many aspects were eventually generalized and are fully configurable at run-time. Each telescope can be separately configured, including its optical layout and properties as well as the camera configuration, how telescope and system trigger conditions are formed, and also how the signals get digitized and recorded. In its current implementation, it is also referred to as the `sim_hessarray` package although it is in no way specific to H.E.S.S. By exchanging a number of configuration files, any other IACT system can be simulated just as well.

Realistic and detailed detector simulations are key features of the `sim_telarray` package but efficiency is just as important. Often, simulation studies require a billion and more events, sometimes with many telescopes in each event – in some studies for CTA [11] close to 100. Full simulation of night-sky background (NSB) and electronic noise in every pixel of every telescope event would be prohibitively slow for such studies. In other cases, e.g. for finding reasonable trigger conditions where random triggers due to night-sky background are at a manageable level, the full simulation of each and every event is unavoidable.

As long as night-sky induced triggers are negligible and most simulated events will not trigger a telescope, `sim_telarray` offers several short-cuts in the simulation which can boost efficiency by large amounts without losing events that would eventually trigger a telescope. These short-cuts require initial full simulations to determine safe lower limits for the numbers of Cherenkov photons and the resulting number of photo-electrons needed to trigger a telescope

(except for NSB-induced triggers). Where the required number of photons – based on the sum of all photon bunches hitting the fiducial sphere – is not met, the simulation can be bypassed completely. Otherwise the optical ray-tracing and photon detection are carried out and the sum of all photo-electrons is compared to the second limit. Only where that is met as well we have to go through the detailed simulation of the electronics response. The difference between complete bypassing and full simulation without much Cherenkov light can be up to 5 orders of magnitude in time, with little more than 0.01 seconds for the full simulation of a H.E.S.S.-I type telescope on a fast CPU core. In real productions, the short-cuts typically result in improvements by factors of 10 to 100.

3.2 Optics simulation

All IACTs to date have segmented reflectors made with mirror tiles of spherical type. The optical ray-tracing in `sim_telarray` fully reflects this current usage, with spherical mirror tiles of round, hexagonal, or square shape. The optical quality of the tiles can be adjusted to laboratory measurement, including variations in focal length or non-perfect surfaces. Also the mirror adjustment, typically performed with star light falling onto the lid of the camera, will have a limited accuracy and is taken into account when every individual mirror tile is configured at program start-up. How well this approach can represent real telescopes is demonstrated in the case of the H.E.S.S. I reflectors, based entirely on mirror quality lab measurements and the measured accuracy in the mirror alignment procedure [12][13], without any free parameters. Not only are the general characteristics of the optical PSF reproduced but also the detailed shapes of star light imaged onto the camera lid [14] (see Figure 6), at least for the zenith angle range where the alignment was carried out. The zenith-angle dependence of the alignment quality, due to dish deformations, can be set as well in order to match measurements or separate finite elements calculations.

The optics is defined by the overall focal length f_{tel} , a table of mirror positions (x_i, y_i) perpendicular to the optical axis, shapes, and sizes as well optional z_i positions and mirror tile focal lengths f_i . If the z_i positions are omitted, mirrors will be positioned following variants of either a Davies-Cotton or parabolic dish shape, taking mechanical accuracies into account. Mirror tiles can have either all the same focal lengths, specific f_i from the table, or automatically optimized f_i derived from the desired dish shape and (x_i, y_i) .

In the case of a parabolic dish, the optimal mirror tiles would clearly be paraboloid segments, while all IACTS so far have been equipped with spherical tiles. The optimum focal lengths of spherical tiles on a parabolic dish can be obtained by calculating the principal (maximum and minimum) radii of

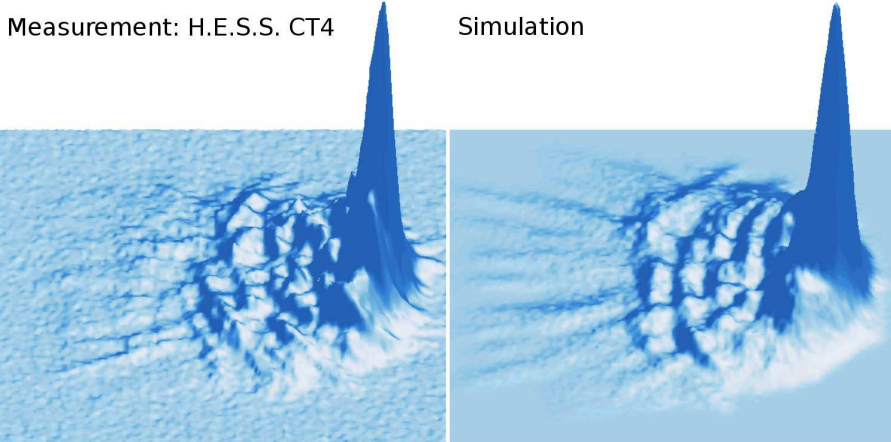


Fig. 6. Measured (left) and simulated (right) distribution of star light imaged onto the lid of a H.E.S.S. camera at an off-axis angle of 2.3° , adapted from [14]. The fields shown are about 10.5 cm (0.40°) wide.

curvature of the paraboloid at the position of the mirror segment. Half the geometric mean, i.e. $0.5 (r_{\min} r_{\max})^{1/2}$, is used for automatically optimized f_i but the simple distance of the mirror tile to the system focus would be reasonable as well, as the two lead to almost the same result. Practical aspects of the mirror production for a real IACT may dictate to build mirror tiles of only a few different focal lengths or even a single focal length, within specifications. The optical ray-tracing of `sim_telarray` is well suited for comparing the optical point-spread functions (PSF) of different designs and optimize the design.

An example study for the H.E.S.S.-2 telescope now under construction is illustrated in Figure 7, demonstrating that the optical PSF is only marginally deteriorated by choosing a single focal length for all mirror tiles.

Since the propagation time of light is included in the optics simulation, the time spread due to non-isochronous mirror configurations is automatically reproduced. While a parabolic dish guarantees the shortest possible Cherenkov pulse durations, different dish shapes may result in a still acceptable time spread while improving the off-axis PSF. The `sim_telarray` program therefore allows for variations of the assumed dish shape with respect to either a Davies-Cotton or parabolic base design. Since the most important aspect here is the radius of curvature of the dish this is largely equivalent also to elliptical intermediate dish shapes.

Mirror tiles can be of hexagonal, square, or circular shape. Since the test for intersection with every mirror tile could be very time consuming in the simulations, a grid scheme somewhat similar to that in the CORSIKA IACT option is applied, this time along the dish onto which the mirror tiles are mounted. A mirror may be associated with one or more grid cells. By intersecting the path

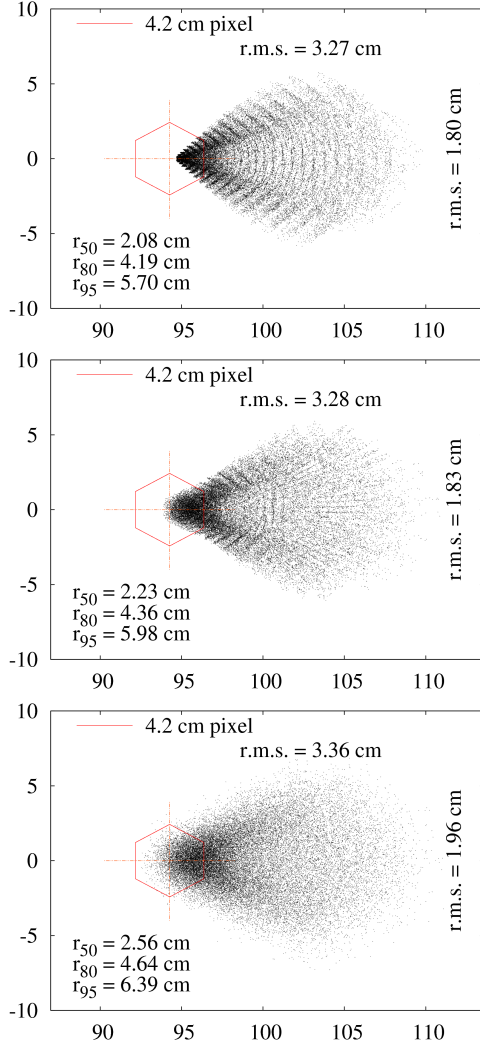


Fig. 7. Study of the point spread function of (Cherenkov) light from a point source at 10 km distance and 1.5° off-axis imaged to the pixel entrance plane in a H.E.S.S.-2 type telescope ($f = 36$ m, coordinates in units of centimetres). The worst case off-axis orientation, along the larger vertical dish diameter, is assumed. Top: ideal mirror alignment and individually adapted mirror tiles. Middle: all mirror tiles of identical focal length. Bottom: in addition with realistic mirror alignment accuracy. R.m.s. widths of the light distributions along radial and transverse directions are indicated in the figures, as well as 50%, 80%, and 95% containment radii. Note the extremely fine pixels of 0.067° .

of the incoming photon with the dish one grid cell gets selected and the detailed intersection has to be evaluated only for the few mirror tiles associated with that cell. Every mirror tile is once set up with random misalignments and misplacements according to realistic specifications. Its actual focal length may randomly vary around the defined or optimized value. The surface is assumed to exhibit some random roughness resulting in a small smearing of the reflected rays.

As an optional feature, not normally used for performance reasons, the support structure for the camera can be included in the ray-tracing, approximated by an arbitrary number of cylinders. This way, the *shadowing* by the camera support structure and by the camera itself and its open lid can be evaluated in detail, taking both incoming and reflected photons into account [12]. For normal production, the shadowing by the support structure is parametrized as a function of the angle w.r.t. the optical axis and only the shadowing by the camera is explicitly included.

In order to make such optical studies possible, and also for realistic tests of the impact of a non-uniform NSB on the shower reconstruction, `sim_telarray` allows to set up additional light sources, normally at infinite distance (stars) but optionally at finite distance to evaluate the imaging of specific positions along a shower axis. For the optical studies the listing of reflected photons can be written to a file. For the shower simulations, the additional stars result in an enhanced noise in the illuminated pixels, for efficiency reasons determined once at program start-up. The average or *direct current* (DC) of stars in the photo tubes – which gets decoupled by high-pass filters in real detectors – is subtracted and not present in the signals.

With mirror tiles aligned to focus star light on the closed lid of the camera, the Cherenkov light from the showers is focused behind the lid, at an offset

$$d = (f^{-1} - D^{-1})^{-1} - f$$

for light emitted at a distance D from the telescope of focal length f . See [15] on possible strategies for optimal focusing on showers.

As a final step of the optics simulation, the angular acceptance of the pixels is taken into account since pixels are typically equipped by Winston cones or such to avoid gaps between neighbouring pixels as far as possible. For practical reasons, this is made part of the photon detection efficiency. As far as the ray-tracing is concerned, it is sufficient to find out which (if any) pixel is hit at the entrance of its Winston cone or similar and optionally if the photo-cathode at the base of the Winston cone is hit directly or not. The shapes of pixel entrance and unobstructed photo-cathode can be hexagonal, square, or circular. A more detailed set-up, activated in the camera configuration file, may include angular acceptance tables, averaged over the pixel area, as obtained from measurements or detailed ray-tracing of the light collectors. Whenever the relevant data is available, the more detailed mode is usually preferred.

3.3 Photon detection

The photon detection probability ε basically depends on the atmospheric transmission T , shadowing factor S by the camera and its support structure, the mirror reflectivity R , the efficiency E of the light concentrator (optionally whether a photon hits a pixel directly onto the photo-cathode or via reflection on the light concentrator), on the quantum efficiency Q of the photo-cathode and finally the collection efficiency C inside the PMT. Most of them are functions of wavelength:

$$\varepsilon(\lambda) = T(\lambda)SR(\lambda)E(\lambda)Q(\lambda)C(\lambda).$$

While fluctuations in the reflectivity of individual mirror tiles are smoothed out, the fluctuations in quantum efficiency have to be taken into account. Such fluctuations in quantum efficiency from PMT to PMT are usually obtained by measuring the photocathode currents of all PMTs induced by a calibrated light source, e.g. the CB (Corning Blue) value provided by the manufacturer. The collection efficiency of typically 80 to 90% is the probability that a photo-electron actually hits the first dynode of a PMT and is effectively multiplied rather than elastically scattered. It can be accounted for in two ways. Either by including it in the detection probability as above and the pulse amplitude distribution at the anode only accounting for photo-electrons multiplied at the first dynode. Or by including the non-amplified photo-electrons in the amplitude distribution of single photo-electrons (*single p.e.*), see Figure 8. For that purpose, the single-p.e. amplitude is randomly drawn according to a table rather than from a normal distribution. The small wavelength dependence of the collection efficiency is a consequence of the photo-electric effect. It may be accounted for by adjusting the quantum efficiency according to

$$\tilde{Q}(\lambda) = Q(\lambda)C(\lambda)/\bar{C},$$

where \bar{C} is the average or effective collection efficiency. In Figure 9 this is illustrated for PMTs evaluated for H.E.S.S.

For a realistic detector response, both the quantum efficiency and the voltage required to achieve the desired gain can vary from PMT to PMT. For simplicity, the same scaling factor is applied to the quantum efficiency at all wavelengths. Variations of the voltage U result in variations of the PMT transit time which is proportional to $1/\sqrt{U}$. The simulation also includes a transit time jitter for individual photo-electrons.

The pixels are permanently exposed to NSB at a level configurable for every pixel (including light of additional bright stars), in units of photo-electrons per

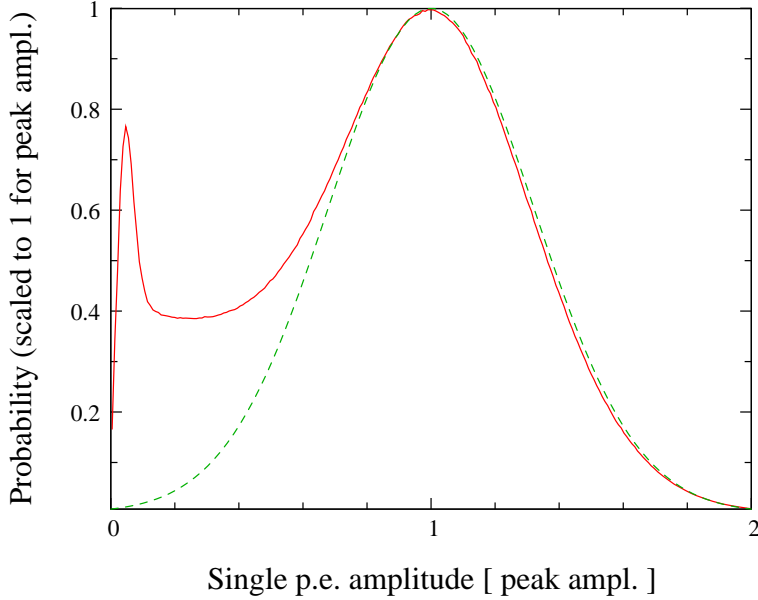


Fig. 8. Single-p.e. amplitude distribution at the PMT anode for the two ways to take a 85% PMT collection efficiency into account. Solid line: collection efficiency included in the amplitude distribution (the mean amplitude is 85% of the amplitude in the peak of the distribution). The distribution here is based on a detailed simulation of the multiplication process in PMTs with parameters fitted to match low-noise measurements between 0.1 and 3 times the peak amplitude. Dashed line: collection efficiency is included with the quantum efficiency and a normal distribution is assumed.

nanosecond. For existing detectors, this number is obtained from the image noise. An utility program is provided for evaluating the impact of different quantum efficiency curves, different mirror reflectivity etc. on the NSB rate, assuming the NSB spectrum measured by Benn and Ellison [17]. In real detectors, the DC (direct current) contributions get decoupled by high-pass filters. In the simulation, the mean amplitude of NSB signals is therefore subtracted from the signal baseline. For every random NSB photo-electron, the corresponding pulse shape with randomized amplitude is added on top of that baseline.

Another important NSB aspect taken into account is the afterpulsing typically induced by ions in the PMT hitting the photo-cathode. These afterpulses typically come hundreds of nanoseconds after the original electron cascade by which the atom was ionized. For Cherenkov photons, the afterpulses will therefore always be well outside the readout window. NSB photons registered hundreds of nanoseconds earlier though can be well responsible for afterpulses within the time window relevant for the trigger and signal readout. The amplitude distribution of afterpulses extends to much larger amplitudes than that of normal signals (see Figure 10). This fact is taken into account by having different single-p.e. amplitude distributions for Cherenkov light and for NSB,

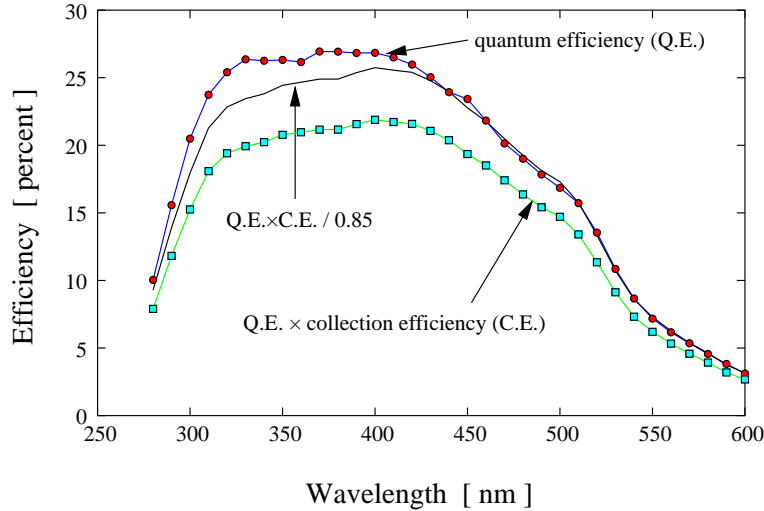


Fig. 9. Quantum efficiency (upper curve), quantum efficiency times collection efficiency (lower curve), and the latter divided by the mean collection efficiency of 85% (middle curve) as evaluated for a sample of PMTs for the H.E.S.S. experiment [16]. The `sim_telarray` program can be either configured to include the mean collection efficiency in the single-p.e. amplitude distribution (together with the middle curve for the effective quantum efficiency) or to include it with the quantum efficiency (using the lower curve).

with the afterpulse amplitude distribution added for the NSB signals only. How important proper accounting for afterpulses can be is demonstrated in Fig. 11.

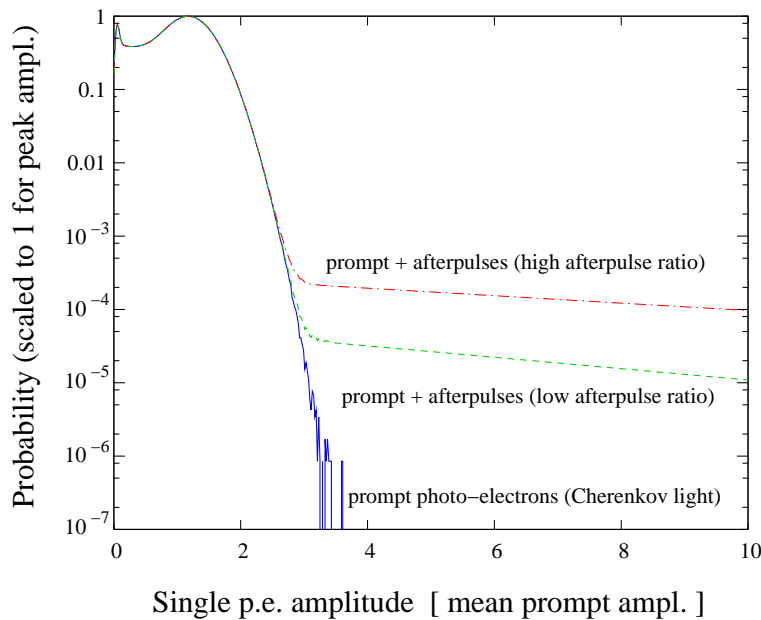


Fig. 10. Amplitude distribution for prompt single-p.e. signals and after including the afterpulses (fits to two types of PMTs, as compared in Figure 11).

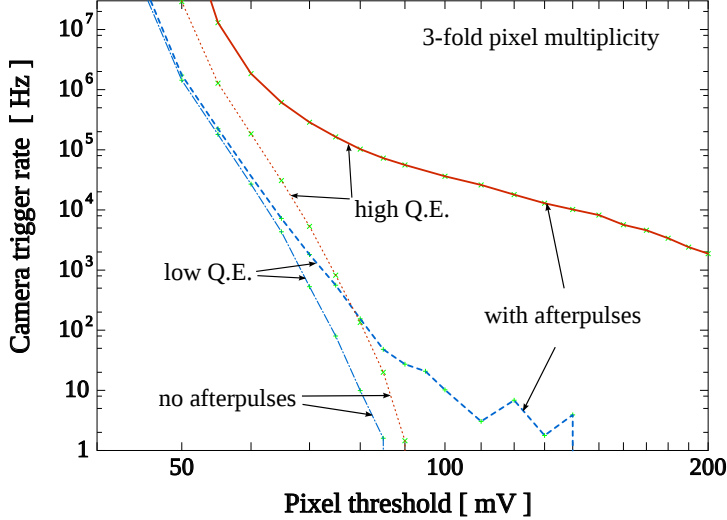


Fig. 11. Example evaluation of PMT specifications for use in a future Cherenkov telescope. One PMT type has a slightly higher quantum efficiency but also a five times higher afterpulse ratio than the other (see Figure 10). Simulations assume a mean single-p.e. amplitude of 23 mV for both and the same night-sky background resulting in random camera triggers (without any Cherenkov light). For the thin dotted and dash-dotted lines the afterpulsing is ignored, resulting in only a small increase in pixel comparator thresholds required with high Q.E. PMTs to achieve the same trigger rate as with low Q.E. PMTs. When afterpulsing is included (thick solid and dashed lines), the higher Q.E. PMT turns out to be unusable, at least with 3-fold pixel coincidences, because the required threshold would be at least three times as large as for the low Q.E. PMT type.

3.4 Electronic signals and trigger

After the photons are ray-traced to the PMT pixels and there may be a chance of triggering of the telescope, based on the number of photo-electrons, detailed simulation of the electronics response is started. Several different pulse shapes are involved. These begin with the pulse shape for a single p.e. at the input of a comparator or discriminator for each pixel. Similar but different pulse shapes apply for each channel in the digitization process. Two ways of having more than one channel per pixel are supported here: different pre-amplifier gains for an enhanced dynamic range (as used with H.E.S.S.) and multiple, phase-shifted FADC modules for achieving a high sampling rate (as used with HEGRA).

For the analogue signal at the comparator or discriminator input, an internal sampling short compared to actual pulse durations is required. Typically, a 250 ps time interval is used for pulses of a few nanoseconds. Where the camera digital electronics should provide only an integrated signal, a sufficiently fine-grained internal sampling is used in the first place and the signal is added up

afterwards. Otherwise the actual sampling of the read-out system is used and the common phase of the digitization (across the whole camera) is randomized with respect to the photon arrival times. For each photo-electron, the pulse shapes are scaled by the random single-p.e. response and shifted according to the photon arrival time plus PMT transit time including a random jitter. All single-p.e. signals from the Cherenkov light as well as the NSB photons are added up. For pixels exposed to too much star light, limits are available when the pixels are disabled in the trigger and when their HV would be turned off to avoid damage.

For a realistic response of the trigger system, the switching behaviour of the comparators or discriminators and the rise and fall times of their output signal – typically on the order of a nanosecond – has to be taken into account, as illustrated in Figure 12. And they will not switch instantly when the signal exceeds the predefined threshold. This can be either achieved by demanding a minimum time-over-threshold or a switching charge (minimum area between pulse shape and threshold level). The `sim_telarray` program even takes possible variations in the output amplitude from device to device – 10% being not uncommon – into account. Since the telescope trigger decision is based (at least effectively) on a second comparator or discriminator decision applied to the sum of pixel logic outputs, this has testable consequences. A fully digital trigger decision would correspond to zero rise and fall times as well as identical amplitudes of all pixel logic outputs. In reality, the signals are so short that the pulse shape of pixel logic outputs should not be ignored. As an example, the – originally unexpected – smooth change in trigger rate of the first H.E.S.S. telescope as a function of the multiplicity threshold could be readily explained by the available simulations, with comparator properties according to manufacturer specifications. This is illustrated in Figure 13.

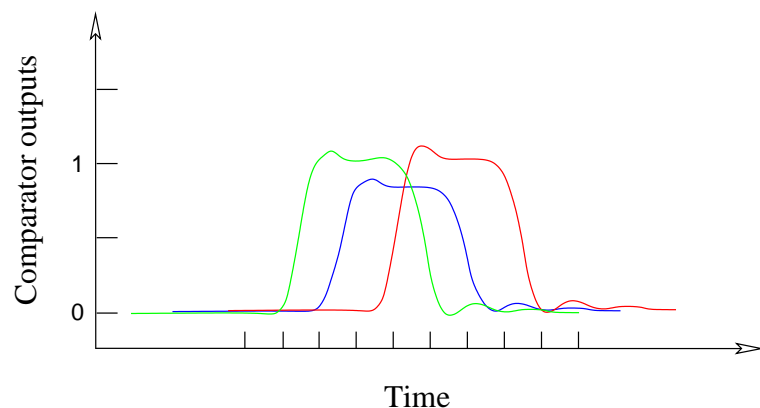


Fig. 12. Three comparator or discriminator output signals partially overlapping in time may or may not be sufficient for a telescope trigger set to a 3-fold multiplicity threshold. Detailed treatment of trigger switching is required.

The telescope trigger logic, i.e. comparator or discriminator outputs from which pixels can be combined to form a telescope trigger, is different for each

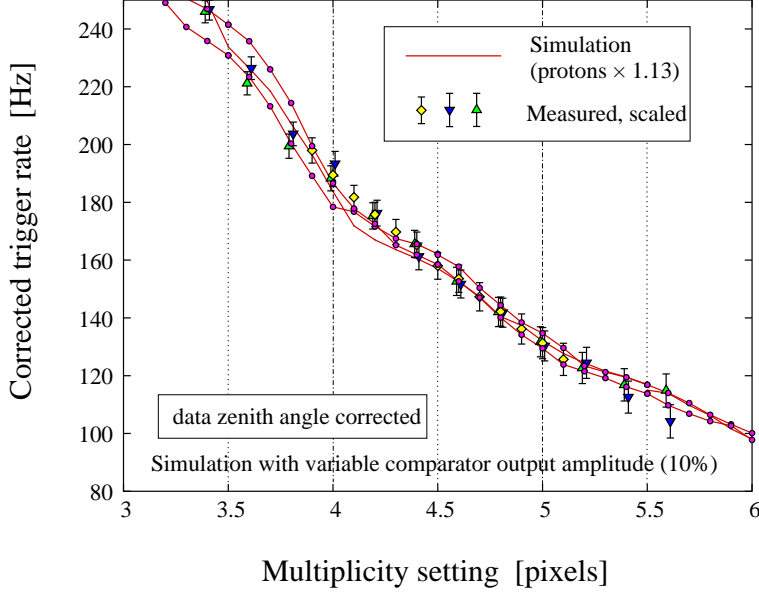


Fig. 13. Telescope trigger rate as a function of the threshold level corresponding to the pixel multiplicity. Data from the first H.E.S.S. telescope [18], taken in different nights and corrected for zenith angle dependence. Simulations including only proton showers were scaled up in absolute rate by a common factor to match the data (no absolute calibration being available at that time). The telescope triggers when the (analogue) sum of the pixel comparator outputs in any *sector* of 64 pixels can switch the sector comparator with programmable threshold. That threshold is shown here in units of the average pixel comparator output, i.e. effectively the number of pixels fired at the same time. Idealized simulations would show steps at integer multiplicity values, while the realistic simulations show only a very modest flattening between integer values. Three sets of simulations were carried out, with random variations of quantum efficiencies, comparator output levels, etc., as indicated by manufacturer specifications.

IACT array. In HEGRA a *next-neighbour* logic was used and in H.E.S.S. a *sector* logic based on 8×8 pixel sectors, while Smart Pixel [19] and other designs differ again. The `sim_telarray` program aims to be fully flexible in this area and its configuration files include lists of all pixel combinations from which a telescope trigger can be formed via a (multiplicity) threshold in the sum of corresponding comparator/discriminator outputs.

The last step in the trigger decision of an IACT array will be the system trigger, usually as a requirement of at least two telescope triggers within a short time window, after correcting for the expected time delay as a function of the system viewing direction and the telescope positions. The required width of the window – typically several 10 ns – depends not only on the fields-of-view of the telescopes but also on the stability of the transmission lines (cable or optical fibres) from the telescopes to the central or distributed system trigger logic. Since random system trigger rates are typically very low and the width of the system trigger time window therefore usually chosen wide enough, any

changes in transmission delays can be ignored by `sim_telarray`. Since the delay times are compensated automatically in `sim_telarray`, the telescope multiplicity and the width of the coincidence time window are usually the only parameters needed. Optionally, `sim_telarray` allows read-out of non-triggered telescopes, as it happened to be the case for the HEGRA IACT array.

3.5 *Telescope raw data and other output data*

The main output data from `sim_telarray` should correspond to what would be recorded from real telescopes (*raw data*) as closely as possible. This can be full *sample-mode* digitized pulse shapes for every pixel or the signal sum over the given integration window. Different types of zero-suppression are possible, like suppression of low-gain channels when the amplitude in corresponding high-gain channels is small or full suppression of pixels with small amplitudes.

The underlying data format is based on the *eventio* machine-independent format, like the CORSIKA IACT output itself but using more and different data block types. Strictly simulation-related data, like the nature, direction, and true energy of the primary particle or the actual displacements of telescope arrays with respect to the nominal core position, are kept separate from the raw data, i.e. in separate data blocks but in the same data stream or file, and can be optionally omitted or filtered out later for realistic data challenges. The data format is largely independent of that used by past and current IACT arrays like HEGRA and H.E.S.S. but conversion to experiment-specific formats is generally straight-forward and provided through utility programs.

Data that is needed for calibration, like conversion from ADC counts to photo-electron numbers, laser/LED flat-fielding, muon-ring efficiency etc. can be derived from full simulations of the various types of calibration runs. The more basic numbers like pedestals, photo-electron conversion factors, and flat-fielding coefficients are also directly provided in the output data. For the pedestals, which may depend on a varying temperature and other things in a real detector, a random ‘measurement’ error with configurable r.m.s. is applied to the reported value.

3.6 *Built-in shower reconstruction and event visualization*

The `sim_telarray` program includes a basic geometrical shower reconstruction, based on second moments (Hillas parameters) and stereoscopic reconstruction methods originally developed for HEGRA. The shower direction is defined by the weighted average of the pair-wise intersection points of Hillas

second-moments major axes in every two-telescope combination with two well-defined images. Only those reconstruction steps are carried out which do not require any look-up of other simulation data. Energy lookup and gamma-hadron-discrimination are thus precluded here. Instead, the reconstruction is oriented towards immediate visualisation of the data. A dedicated Postscript-generator for very compact plot output was developed for that purpose. See Figure 14 for an example.

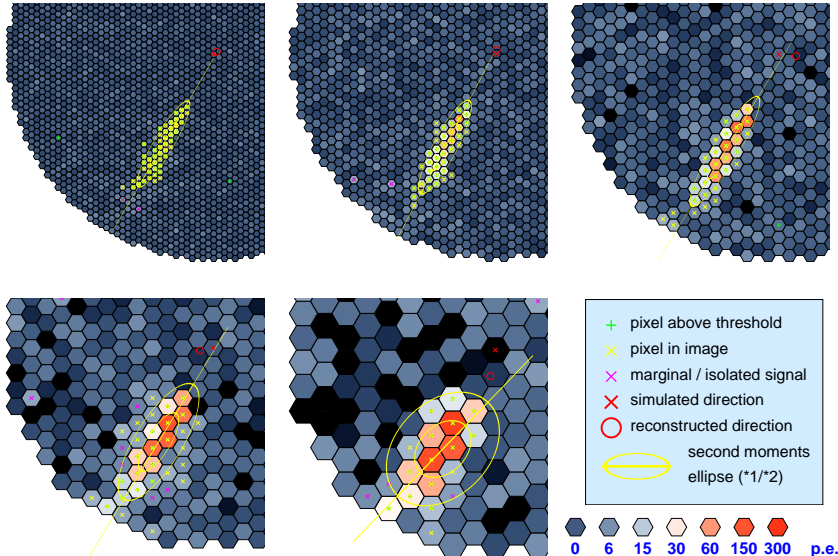


Fig. 14. Example of the `sim_telarray` event visualisation, showing the same shower (a γ -shower of 460 GeV energy at 190 m core distance) in telescopes with different pixel sizes of 0.07 to 0.28°, in a 9-telescope array evaluated for the CTA project [11]. For clarity, only part of the field-of-view of one and the same of the nine telescopes is shown for each pixel size. The second moments ellipses are shown at one and two times their actual size, with the major axes drawn up to four times their actual length. Reconstructed and actual shower directions are indicated by the small circles and crosses near the camera centres, respectively.

4 Conclusions and outlook

The CORSIKA program with the IACT/ATMO extensions aims to provide the most detailed simulation of air showers and the production of atmospheric Cherenkov light, both for imaging and non-imaging detectors. For efficiency reasons not every possible detail is normally used, like the wavelength dependence of the index of refraction, but is available on demand. A variety of options are at hand to adapt the level of detail and performance as needed for specific applications. Parts of the photon detection probability can be applied within CORSIKA or can be provided by the second simulation stage, the detector simulation. The machine- and compiler-independent *eventio* data format allows for a variety of schemes. The IACT extension, normally but not

necessarily using this flexible data format, allows treatment of the largest telescope or detector arrays envisaged for coming generations of atmospheric Cherenkov experiments or observatories. It is part of the standard CORSIKA distribution for several years now.

For the second stage of the simulation process, a dedicated program for imaging telescopes with tessellated primary mirrors, termed `sim_telarray`, aims to provide the greatest level of detail in the simulation of all optical and electronics components involved in the measurement process. At the same time, `sim_telarray` is highly efficient. The *eventio* data from the CORSIKA IACT option can be piped concurrently into several `sim_telarray` processes, each with a different configuration, while avoiding I/O bottlenecks on large computer clusters.

The simulation results from `sim_telarray` can be either written directly into an experiment-specific format, as initially done with the HEGRA IACT system, or into a more generic, *eventio*-based format. The resulting data can be analysed directly from the latter format or converted into experiment-specific formats, e.g. the H.E.S.S. data format, and then analysed with the same software as measured data.

A wide range of cross checks with measured data – mainly by H.E.S.S. – confirms that CORSIKA and `sim_telarray` can reproduce the data extremely well, for newly commissioned telescopes just based on pre-production lab measurements of mirror qualities, quantum efficiencies and so on. Examples of that include the optical PSF [13], the intensity, ring radius, and ring width of muon ring images [20], image shapes of gamma and background showers as well as the reconstructed shower PSF for point-like gamma-ray sources [21, 22], as well as the trigger rates [18]. After commissioning, H.E.S.S. simulations only had to be adapted to the slowly degrading optical throughput of the telescopes.

Future developments in `sim_telarray` may include non-spherical mirror tiles or secondary mirrors, and extensions to the photon detection code, as detectors with novel properties come into operation. Since the aim is to provide data like a real instrument, more capabilities of future read-out systems, like advanced post-processing in FPGAs which may include peak finding and shape analysis, are among the most recent additions.

The CORSIKA program together with the IACT/ATMO package is available from Forschungszentrum Karlsruhe. For details see <http://www-ik.fzk.de/corsika/>.

The `sim_telarray` program is available on request from the author. A release under an open source licence is foreseen.

Acknowledgements

It is a pleasure to thank D. Heck and T. Pierog for the development and the continued maintenance of CORSIKA in the first place but also for the seamless integration of Cherenkov emission and the IACT/ATMO extensions into CORSIKA and its build process. Quite a number of other people have made important contributions to the variety of options available for Cherenkov light emission in CORSIKA. The `sim_telarray` program has seen extensive testing with data from the HEGRA and H.E.S.S. experiments. A large effort by many colleagues went into the data by these experiments as a whole and also into the many lab and field measurements which were useful for the various configuration files, from quantum efficiencies and mirror reflectivities over pulse shapes, detailed single-p.e. measurements to mirror point spread functions and mirror alignment etc.

References

- [1] D. Heck, et al., CORSIKA: A Monte Carlo code to simulate extensive air showers, Tech. Rep. FZKA 6019, Forschungszentrum Karlsruhe (1998).
- [2] S. Martinez, F. Arqueros, V. Fonseca, A. Karle, E. Lorenz, R. Plaga, M. Rozanska, Nucl. Instr. and Meth. A 357 (1995) 567.
- [3] F. Aharonian, et al., H.E.S.S. letter of intent, Tech. rep. (1997).
URL <http://www.mpi-hd.mpg.de/HESS/>
- [4] D. Heck, T. Pierog, Extensive air shower simulation with CORSIKA: A user's guide, Tech. rep., Forschungszentrum Karlsruhe (2007).
- [5] W. Nelson, H. Hirayama, D. Rogers, The EGS4 code system, Tech. Rep. SLAC 265, Stanford Linear Accelerator Center (1985).
- [6] P. E. Ciddor, Appl. Optics 35 (1996) 1566.
- [7] B. Rosenbaum, Tech. Rep. NASA TN D-6209, NASA (1971).
- [8] K. Bernlöhner, et al., Nucl. Instr. and Meth. A 369 (1996) 284.
- [9] A. Daum, et al., Astropart. Phys. 8 (1997) 1.
- [10] K. Bernlöhner, Astropart. Phys. 12 (2000) 253.
- [11] K. Bernlöhner, E. Carmona, et al., MC simulation and layout studies for a future Cherenov Telescope Array, in: Proc. of the 30th International Cosmic Ray Conference, 2007.
- [12] K. Bernlöhner, et al., Astropart. Phys. 20 (2003) 111.
- [13] R. Cornils, et al., Astropart. Phys. 20 (2003) 129.
- [14] R. Cornils, Ph.D. thesis, University of Hamburg (2006).
- [15] W. Hofmann, J.Phys. G: Nucl. Part. Phys. 27 (2001) 933.
- [16] A. Koch, A. Kohnle, private comm. (2000).
- [17] C. Benn, S. Ellison, New Astr. Rev. (1998) 503.
- [18] S. Funk, et al., Astropart. Phys. 22 (2004) 285.

- [19] G. Hermann, et al., A Smart Pixel camera for future Cherenkov telescopes, in: Proc. Conf. Towards a Network of Atmospheric Cherenkov Detectors VII, 2005, arXiv:astro-ph/0511519.
- [20] O. Bolz, Ph.D. thesis, University of Heidelberg (2004).
- [21] F. Aharonian, et al., *Astron. Astrophys.* 457 (2006) 899.
- [22] F. Aharonian, et al., *Astron. Astrophys.* 430 (2005) 865.